Supplementary Information (SI) for Energy & Environmental Science.

# Data−driven Design of Advanced Magnesium−Battery Electrolyte via Dynamic Solvation Models

Ruimin Li[1,2], Wanyu Zhao[2*], Zhengqing Fan[2], Meng Zhang[2], Jiayi Li[2], Rushuai Li[2], Zhijun Zuo[1*], Xiaowei Yang[2*]

[1] State Key Laboratory of Clean and Efficient Coal Utilization, Taiyuan University of Technology, Taiyuan, 030024, P. R. China.

[2] School of Chemistry and Chemical Engineering, Shanghai Jiao Tong University, Shanghai, 200240, P. R. China.

* Corresponding author:

wanyuzhao@sjtu.edu.cn; zuozhijun@tyut.edu.cn; yangxw@sjtu.edu.cn

## I. Supporting Text

## 1. Methods

### 1.1 Electrolyte preparation and electrochemical measurement

We selected 30 sets of electrolyte formulations in RMBs for electrochemical measurements. $Mg(TFSI)_2$ (99.5%, DoDo) was dried at 200 °C under vacuum for 24 hours before using. The solvents were dried overnight with 3 Angstrom molecular sieves and then stored in the glove box before use. The 0.5 M $Mg(TFSI)_2$/solvent electrolytes were prepared by dissolving dried $Mg(TFSI)_2$ into the solvents. Galvanostatic cycling of Mg symmetric cells was performed with the 30 electrolyte formulations at a current density of 0.1 mA $cm^{-2}$ (Neware, CT4008).

### 1.2 Computational study

1.2.1 Classic molecular dynamic(cMD) simulations:

All the classic molecular dynamic simulations conducted in this work were performed using the Large–scale Atomic/Molecular Massively Parallel Simulator (LAMMPS, http://lammps.sandia.gov). The compositions of electrolytes are listed in Table S1. OPLS–AA[1] parameters with 1.14*CMIA partial atomic charges were generated by LigParGen[2-4] for the Organic solvent molecules.[5] The charges and force fields for TFSI anions in the electrolytes were taken from previous publications.[6] The OPLSAA force field developed by Jorgensen was used for $Mg^{2+}$ ions.[7] To get the electrolyte structure, isothermalisobaric (NPT) ensemble runs were first performed at 330 K for 2 ns and then 298 K for 2 ns to ensure the equilibrium salt dissociation. Then, 15 ns canonical (NVT) ensemble simulations were performed, and the last 10 ns (sampled every 0.5 ns) were analyzed using Python codes to count the number of anions and solvent molecules surrounding each $Mg^{2+}$ and to calculate the percentages of all solvation structures. 7.5 ns (sampled every 0.5 ns) long canonical (NVT) ensemble runs were performed for mean square displacement (MSD) curves to determine the diffusion coefficients of $Mg^{2+}$, $TFSI^{-}$, and $OTF^{-}$.

$$D = lim_{t \to \infty} < |r(t) - r(0)|^2 > /dt$$

Where $d$ represents the spatial dimension of diffusion, which is 3 in bulk solution systems. $t$ denotes the diffusion time. To reduce experimental errors, the value of $D$ is averaged 15 simulation runs.

### 1.2.2 Density functional theory (DFT) calculations:

Density functional theory (DFT) calculations for geometry optimization were conducted by Gaussian 16 software package.[8] Geometry optimizations and energy calculations were performed using B3LYP/6–311G(d,p),[9] and the convergence tolerance quality was the default. The solvation effect was considered with the universal solvation model of SMD.[10] Based on the optimized structures, the highest occupied molecular orbital (HOMO), the lowest unoccupied molecular orbital (LUMO) energy level, and corresponding atomic orbital components were analyzed using the Natural Bond Orbitals (NBO) theory.[11] The electrostatic potential (ESP) of the anions was analyzed by using Multiwfn software.[12] The binding energy ($E_b$) of solvation structure was calculated as:

$$E_b = E_{x-y} - E_x - E_y$$

where $E_{x-y}$ is the total energy of the $Mg^{2+}$ solvation structure, and $E_x$ and $E_y$ are the energies of components x and y, respectively.

## 1.3 Machine learning analysis

### 1.3.1 Databases and feature selection

Three databases comprising 6,030 solvation structures were established, as shown in Database S1 (Supporting Information). Database1, Database2, and Database3 correspond to “composition”, “solvation”, and “migration” machine learning, respectively. The outputs for all databases are the overpotential and cycle life of experimentally tested 0.5 M $Mg(TFSI)_2$ electrolyte formulations. For composition ML, we obtained feature values from 30 simulated electrolyte formulations using MD. To reduce statistical error, one frame was taken every 0.5 ns over a 10 ns simulation, and the average solvation structure proportion was calculated (Figure S11). Based on the integer part of the sum, the decimal part was dynamically adjusted to ensure that the top 100 solvation structures for each electrolyte formulation were selected. The corresponding charges, anion, and molecular structure features (including the number of atoms, atom ratios, types of functional groups, etc., totaling 62 features) were used to construct Database1, comprising 3,000 solvation structures. For solvation ML, Database1 was divided into 58 coordination structures based on the coordination number of solvents, additives, and anions. The percentage of each coordination structure was used as the feature value to construct Database2. For migration ML, Database3 was constructed from the diffusion coefficients of $Mg^{2+}$ and $TFSI^-$ (Figure S12), the binding energy of $Mg^{2+}$ solvation structures, the average bond lengths of $Mg^{2+}$ coordinated with $TFSI^-$ and solvent, the energy gap (HOMO–LUMO), and the dielectric constant. All descriptors and their concrete meanings are listed in Table S2.

### 1.3.2 Machine learning methods

All machine learning algorithm implementations come from the scikit–learn package,[13] including kernel ridge regression (KRR),[14, 15] k–nearest neighbor (KNN),[16] random forest (RF),[17, 18] extreme gradient boosting (XGBOOST),[19] and neural networks (NN). Five–fold cross–validation (CV) is used for model selection. Multiple algorithms are evaluated for mean absolute error (MAE), mean squared error (MSE), and root mean square error (RMSE) values on the output of overpotential and cycle life in "composition", "solvation", and "migration" machine learning (Table S3, S4, and S5). The MAE, MSE and RMSE can be defined as follows:

$$MAE(y,\hat{y}) = \frac{1}{n}\sum_{i=1}^{n}|y_i - \hat{y}_i|$$

$$MSE(y,\hat{y}) = \frac{1}{n}\sum_{i=1}^{n}(y_i - \hat{y}_i)^2$$

$$RMSE(y,\hat{y}) = \sqrt{\frac{1}{n}\sum_{i=1}^{n}(y_i - \hat{y}_i)^2}$$

Where $\hat{y}_i$ denotes the predicted value of the $i$–th sample, $y_i$ denotes the corresponding ground–truth for total n samples, $\bar{y}$ denotes $\frac{1}{n}\sum_{i=1}^{n}y_i$. The MAE, MSE and RMSE values should be as small as possible. Additionally, we also employed shapley additive explanations (SHAP) to investigate the contribution of each feature to ML models' output[20, 21] ( Figure S2, S5, and S7). SHAP was implemented by using SHAP Python library (https://github.com/slundberg/shap).

## 1.4 Material Characterization

The microstructure were characterized using scanning electron microscopy (SEM, FEI Apreo 2S), energy dispersive X–ray spectroscopy (EDS) and transmission electron microscopy (TEM, Talos F200X G2).

## II. Supporting Tables

Table S1. Mg salt and solvent details.

| abbreviation | Name | CAS number | SMILES |
|---|---|---|---|
| Mg(TFSI)$_2$ | Magnesium bis(trifluoromethylsulfonyl)imide | 133395-16-1 | C(F)(F)(F)S(=O)(=O)[N-]S(=O)(=O)C(F)(F)F.C(F)(F)(F)S(=O)(=O)[N- |
| Mg(OTF)$_2$ | Magnesium trifluoromethanesulfonate | 60871-83-2 | C(F)(F)(F)S(=O)(=O)[O-].C(F)(F)(F)S(=O)(=O)[O-].[Mg+2] |
| DME | 1,2-dimethoxyethane | 110-71-4 | COCCOC |
| PC | Propylene carbonate | 108-32-7 | CC1COC(=O)O1 |
| EMC | Ethyl Methyl Carbonate | 623-53-0 | CCOC(=O)OC |
| G2 | Diethylene Glycol Dimethyl Ether | 111-96-6 | COCCOCCOC |
| G3 | Triethylene glycol monomethyl ether | 112-35-6 | COCCOCCOCCO |
| G4 | tetraethylene glycol dimethyl ether | 143-24-8 | COCCOCCOCCOCCOC |
| NMA | N-Methylacetamide | 79-16-3 | CC(=O)NC |
| TMP | Trimethyl phosphate | 512-56-1 | COP(=O)(OC)OC |
| NETEN | N-Ethylethylenediamine | 110-72-5 | CCNCCN |

| abbreviation | Name | CAS number | SMILES |
|---|---|---|---|
| DBP | Dibutyl Phosphate | 107-66-4 | CCCCOP(=O)(O)OCCCC |
| TMPhite | Trimethyl phosphite | 121-45-9 | COP(OC)OC |
| DFE | 2,2-Difluoroethylamine | 671-709-6 | C(C(F)F)N |
| TMEN | N,N,N',N'-Tetramethylethylenediamine | 110-18-9 | CN(C)CCN(C)C |
| MMEN | N-methyl-1,2-ethanediamine | 109-81-9 | CNCCN |
| ACR | Acrylamide | 79-06-1 | C=CC(=O)N |
| TMSP | Tris(trimethylsilyl) phosphate | 10497-05-9 | C[Si](C)(C)OP(=O)(O[Si](C)(C)C)O[Si](C)(C)C |
| DAB | 1,4-Diaminobutane | 110-60-1 | C(CCN)CN |
| HMDS | Hexamethyldisilazane | 999-97-3 | C[Si](C)(C)N[Si](C)(C)C |
| 1,4DX | 1,4-Dioxane | 123-91-1 | C1COCCO1 |
| TFE | 2,2,2-Trifluoroethylamine | 753-90-2 | C(C(F)(F)F)N |

Table S2. Composition of 36 electrolyte formulations in cMD.

| | $Mg^{2+}$ | anion | sI | sII | sIII |
|---|---|---|---|---|---|
| 1 | 50 | TFSI$^-$: 100 | DME: 962 | / | / |
| 2 | 50 | TFSI$^-$: 100 | DME: 962 | DBP: 85 | / |
| 3 | 50 | TFSI$^-$: 100 | DME: 962 | TMPhite: 85 | / |
| 4 | 50 | TFSI$^-$: 100 | DME: 962 | TMP: 85 | / |
| 5 | 50 | TFSI$^-$: 100 | DME: 962 | TMP: 255 | / |
| 6 | 50 | TFSI$^-$: 100 | DME: 962 | DFE: 325 | / |
| 7 | 50 | TFSI$^-$: 100 | DME: 962 | NETEN: 250 | / |
| 8 | 50 | TFSI$^-$: 100 | DME: 962 | TMEN: 250 | / |
| 9 | 50 | TFSI$^-$: 100 | DME: 962 | MMEN: 250 | / |
| 10 | 50 | TFSI$^-$: 100 | DME: 962 | ACR: 50 | / |
| 11 | 50 | TFSI$^-$: 100 | DME: 962 | TMSP: 30 | / |
| 12 | 50 | TFSI$^-$: 100 | PC: 1180 | / | / |
| 13 | 50 | TFSI$^-$: 100 | PC: 1180 | DFE: 325 | / |
| 14 | 50 | TFSI$^-$: 100 | PC: 1180 | NETEN: 250 | / |
| 15 | 50 | TFSI$^-$: 100 | PC: 1180 | TMEN: 250 | / |
| 16 | 50 | TFSI$^-$: 100 | PC: 1180 | MMEN: 250 | / |
| 17 | 50 | TFSI$^-$: 100 | PC: 1180 | DAB: 250 | / |
| 18 | 50 | TFSI$^-$: 100 | PC: 1180 | HMDS: 48 | / |
| 19 | 50 | TFSI$^-$: 100 | EMC: 970 | / | / |
| 20 | 50 | TFSI$^-$: 100 | EMC: 970 | TMP: 80 | / |
| 21 | 50 | TFSI$^-$: 100 | EMC: 970 | NETEN: 250 | / |
| 22 | 50 | TFSI$^-$: 100 | G2: 700 | / | / |
| 23 | 50 | TFSI$^-$: 100 | G2: 700 | TMP: 128 | / |
| 24 | 50 | TFSI$^-$: 100 | G2: 700 | TMP:128 | 1,4DX: 59 |
| 25 | 50 | TFSI$^-$: 100 | G3: 536 | / | / |
| 26 | 50 | TFSI$^-$: 100 | G3: 536 | NETEN: 250 | / |
| 27 | 50 | TFSI$^-$: 100 | G3: 536 | TMP: 80 | / |
| 28 | 50 | TFSI$^-$: 100 | NMA: 1300 | HMDS: 480 | / |
| 29 | 50 | TFSI$^-$: 100 | G4: 454 | / | / |
| 30 | 50 | TFSI$^-$: 100 | TMP: 855 | / | / |
| 31 | 10 | TFSI$^-$: 20 | NETEN: 471 | TMP: 434 | / |
| 32 | 10 | TFSI$^-$: 20 | NETEN: 471 | DFE: 709 | / |
| 33 | 10 | TFSI$^-$: 20 | NETEN: 471 | TFE: 625 | / |
| 34 | 10 | OTF$^-$: 20 | NETEN: 471 | TMP: 434 | / |
| 35 | 10 | OTF$^-$: 20 | NETEN: 471 | DFE: 709 | / |
| 36 | 10 | OTF$^-$: 20 | NETEN: 471 | TFE: 625 | / |

Table S3. Descriptors and concrete meanings in machine learning.

| Composition ML | | Solvation ML | | Migration ML | |
|---|---|---|---|---|---|
| description | Nomenclature | description | Nomenclature | description | Nomenclature |
| Number of elements in the solvent and additives | sEn | Number of solvent | solIn | Average bond length between $Mg^{2+}$ and the coordination atoms | Bond length |
| Number of elements in the anions | aEn | Number of additive 1 | solIIn | Binding energy between $Mg^{2+}$ and solvent/ $TFSI^{-}$ | Binding energy |
| Functional groups of solvent and additives | sF | Number of additive 2 | solIIIn | HOMO–LUMO of solvation structure | Energy gap |
| Functional groups of anions | aF | Number of anions | anin | Dielectric constant of solvent and additives | Dielectric constant |
| Ratio of elements in the solvent and additives | sE1E2 | / | / | Diffusion coefficient of $Mg^{2+}$ | D_Mg |
| Ratio of elements in the anions | aE1E2 | / | / | Diffusion coefficient of $TFSI^{-}$ | D_TFSI |
| Charge of the solvation structure | charge | / | / | / | / |

Table S4. Multiple algorithms are evaluated for MAE, MSE, and RMSE values on output of overpotential and cycle life in composition ML.

| | overpotential (test set) | | | cycle life (test set) | | |
|---|---|---|---|---|---|---|
| | MAE | MSE | RMSE | MAE | MSE | RMSE |
| KRR | 0.490 | 0.679 | 0.824 | 1.736 | 8.122 | 2.850 |
| KNN | 0.483 | 0.728 | 0.853 | 0.483 | 0.728 | 0.853 |
| RF | 0.482 | 0.667 | 0.817 | 1.723 | 7.880 | 2.807 |
| XGBOOST | 0.478 | 0.666 | 0.816 | 1.716 | 7.902 | 2.811 |
| NN | 0.502 | 0.678 | 0.823 | 1.899 | 8.139 | 2.853 |

Table S5. Multiple algorithms are evaluated for MAE, MSE, and RMSE values on output of overpotential and cycle life in solvation ML.

| | overpotential (test set) | | | cycle life (test set) | | |
|---|---|---|---|---|---|---|
| | MAE | MSE | RMSE | MAE | MSE | RMSE |
| KRR | 1.231 | 2.071 | 1.439 | 3.198 | 22.718 | 4.766 |
| KNN | 0.990 | 1.616 | 1.271 | 4.563 | 35.406 | 5.950 |
| RF | 0.782 | 0.768 | 0.876 | 2.780 | 10.475 | 3.237 |
| XGBOOST | 0.797 | 1.033 | 1.017 | 3.282 | 15.841 | 3.980 |
| NN | 4.569 | 31.829 | 5.642 | 5.292 | 37.744 | 6.144 |

Table S6. Multiple algorithms are evaluated for MAE, MSE, and RMSE values on output of overpotential and cycle life in migration ML.

| | overpotential (test set) | | | cycle life (test set) | | |
|---|---|---|---|---|---|---|
| | MAE | MSE | RMSE | MAE | MSE | RMSE |
| KRR | 0.251 | 0.201 | 0.448 | 0.733 | 1.774 | 1.332 |
| KNN | 0.022 | 0.053 | 0.230 | 0.041 | 0.300 | 0.548 |
| RF | 0.005 | 0.001 | 0.033 | 0.010 | 0.004 | 0.064 |
| XGBOOST | 0.001 | 0.0001 | 0.012 | 0.005 | 0.004 | 0.062 |
| NN | 0.054 | 0.023 | 0.151 | 0.137 | 0.300 | 0.548 |

## III. Supporting Figures

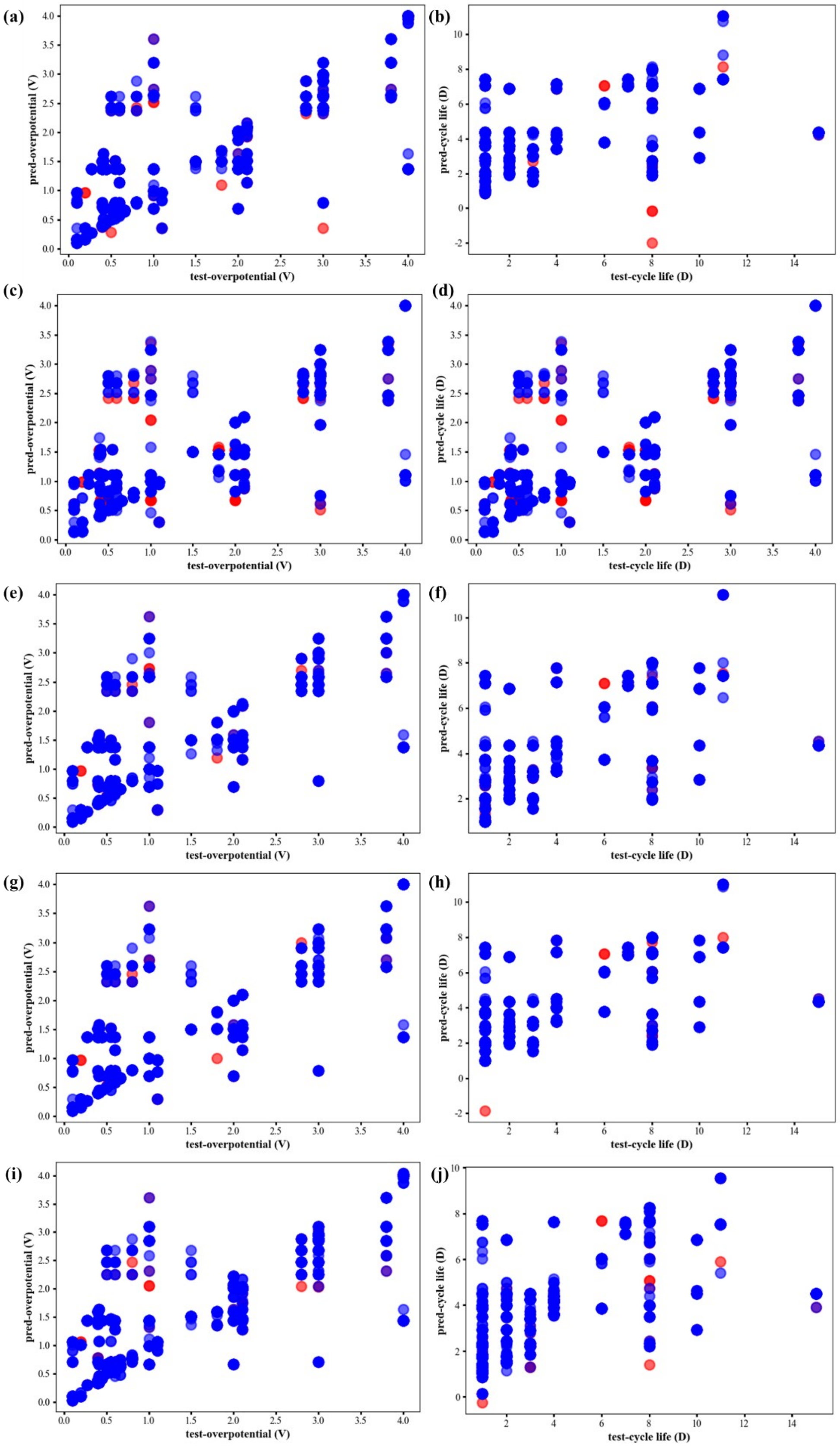

Figure S1. Plots of true and predicted values of KRR(a–b), KNN(c–d), RF(e–f), XGBOOST(g–h) and NN(i–j) model training on composition ML database.

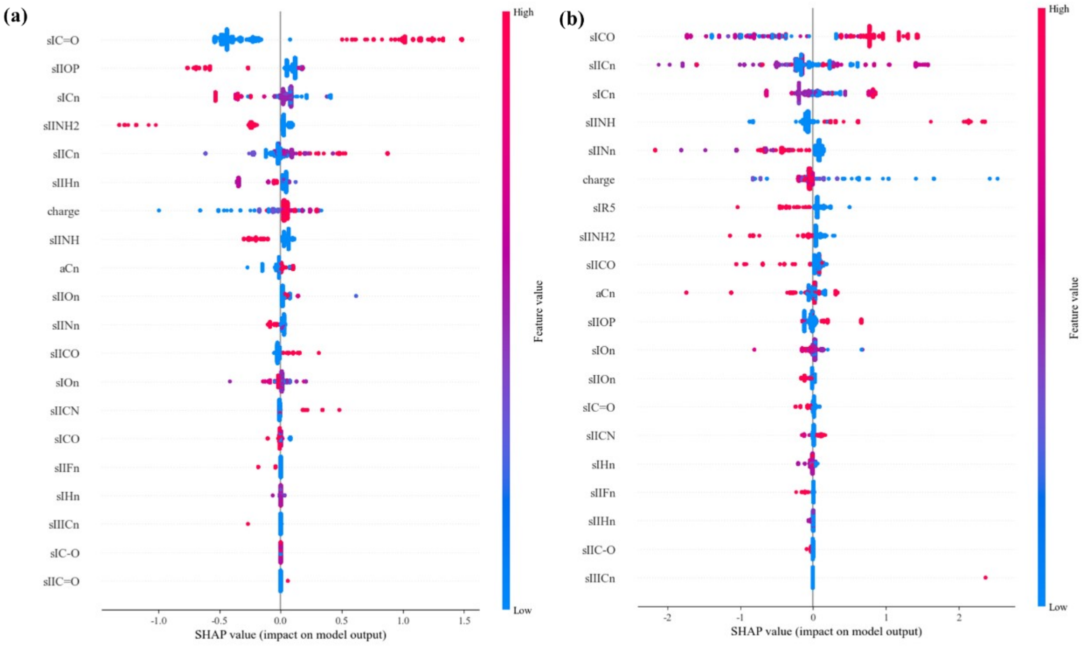

Figure S2. Shaply sorting of XGBOOST model training on a composition ML database with outputs of overpotential (a) and cycle life (b).

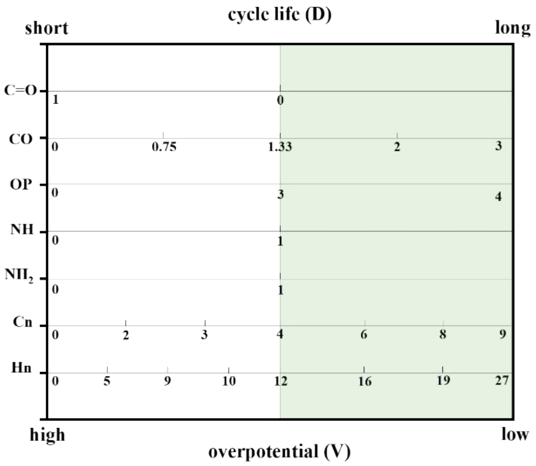

Figure S3. Chemical structure features of composition ML based on electrochemical performance.

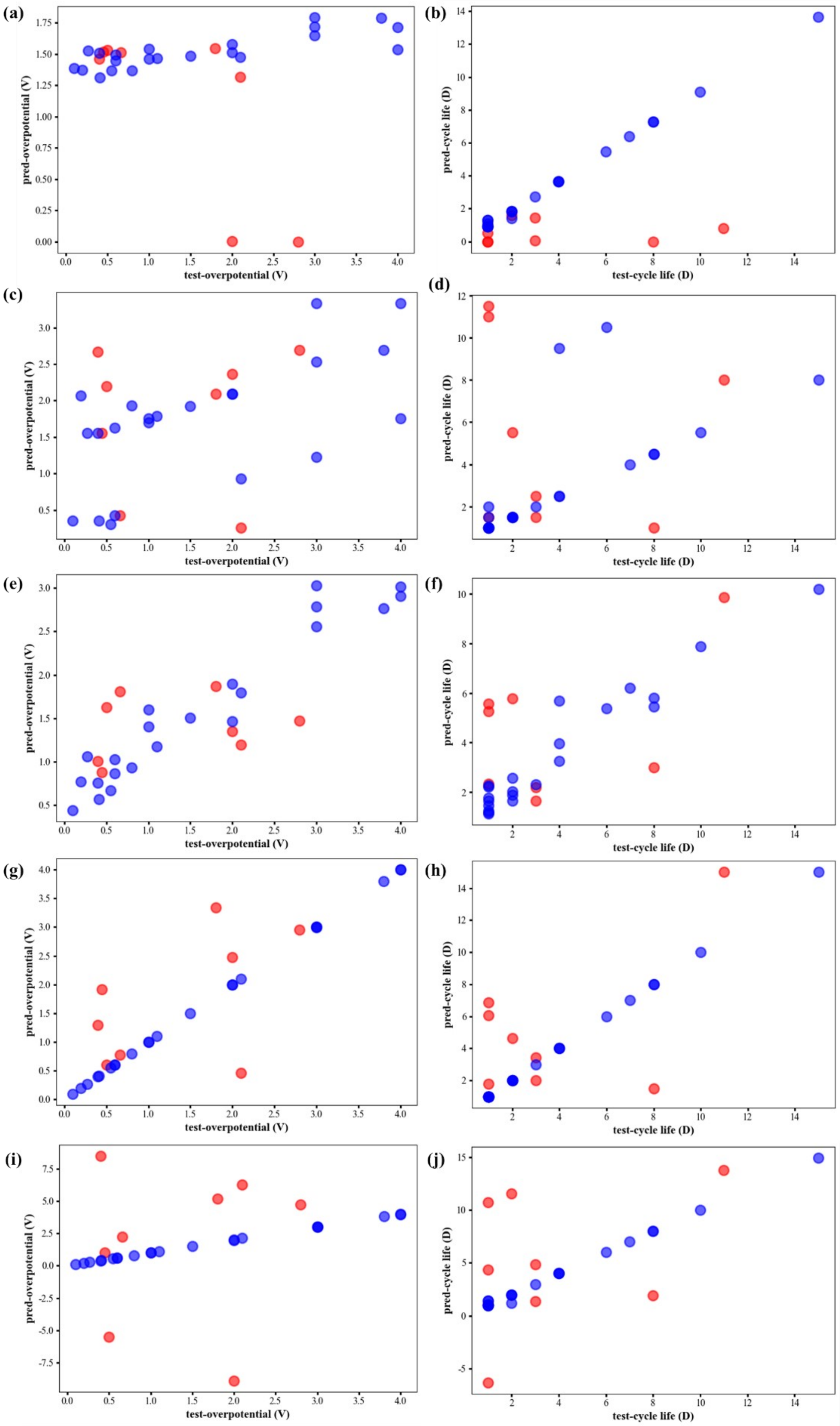

Figure S4. Plots of true and predicted values of KRR(a–b), KNN(c–d), RF(e–f), XGBOOST(g–h) and NN(i–j) model training on solvation ML database.

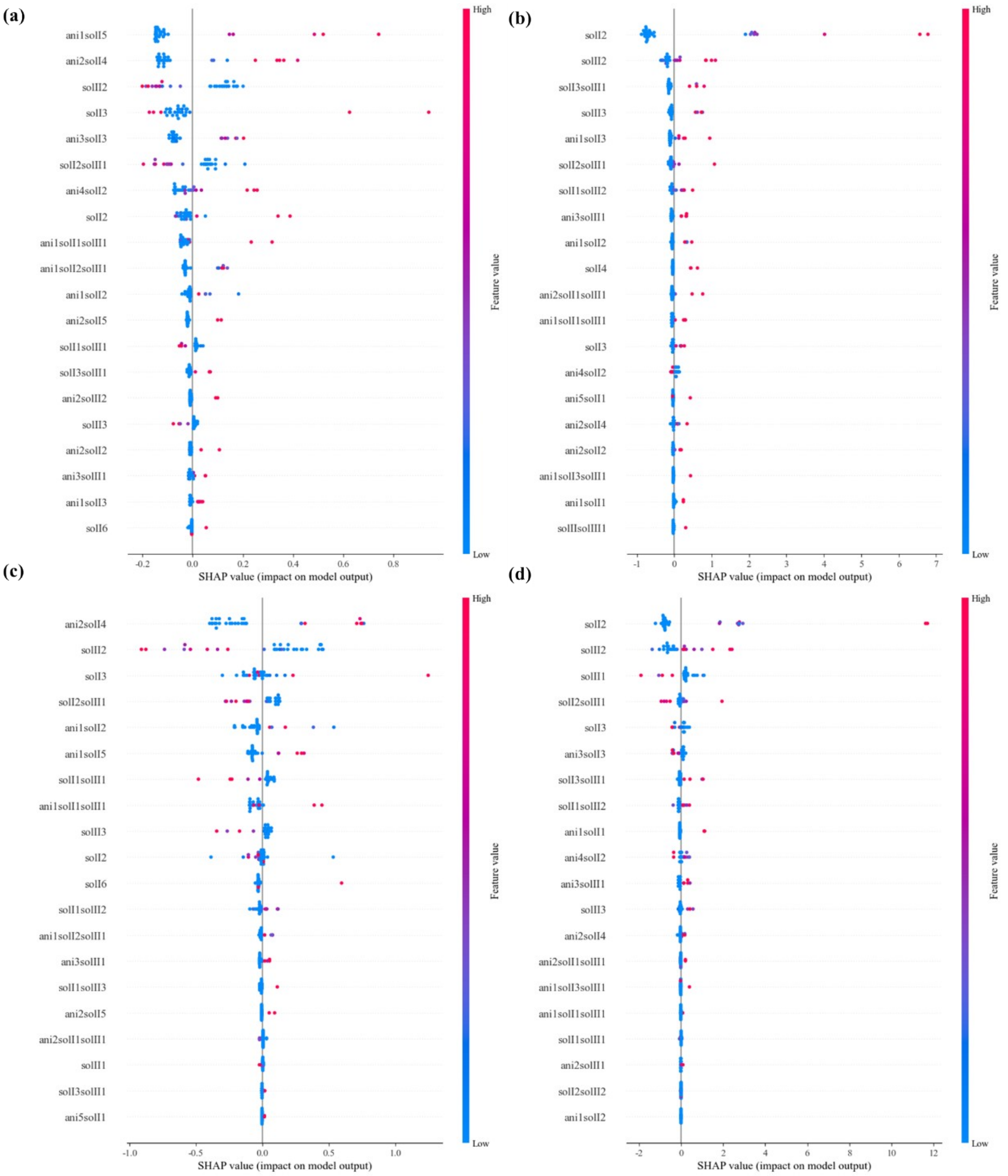

Figure S5. Shaply ordering of RF (a–b) and XGBOOST (c–d) models training on solvation ML database with outputs of overpotential and cycle life.

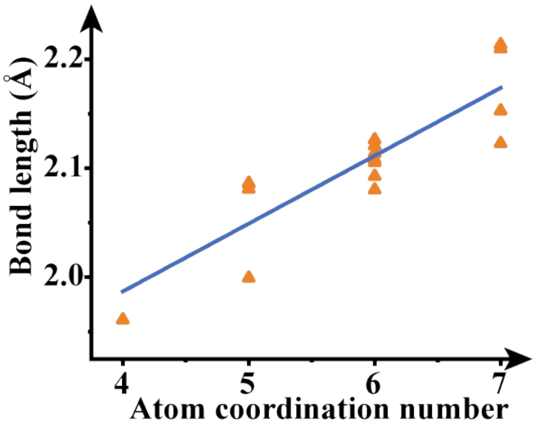

Figure S6. Distribution of atom coordination numbers and average bond lengths in CIP clusters with ligand CN of 2, 3, and 4.

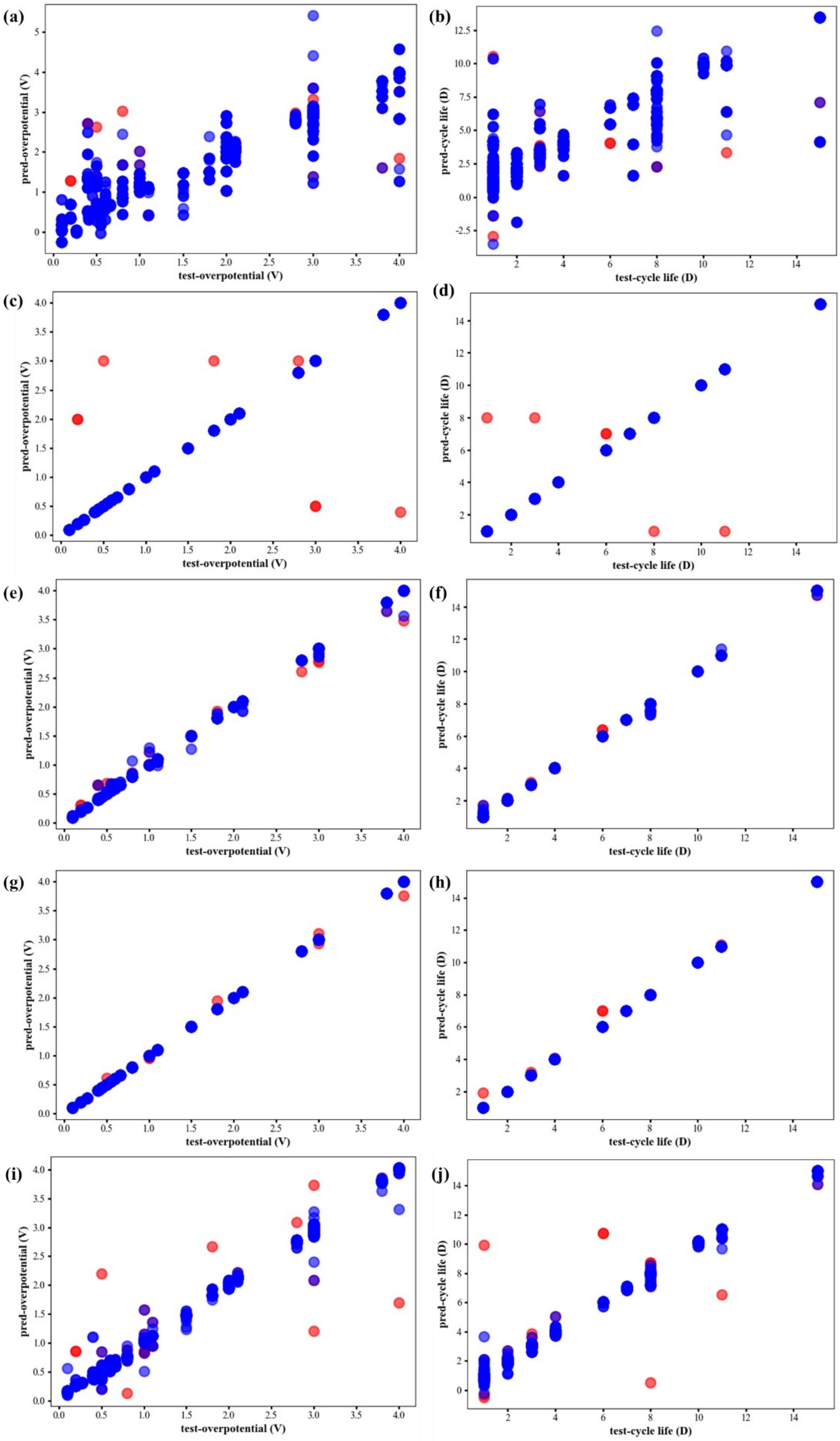

Figure S7. Plots of true and predicted values of KRR(a–b), KNN(c–d), RF(e–f)

XGBOOST(g–h) and NN(i–j) model training on migration ML database.

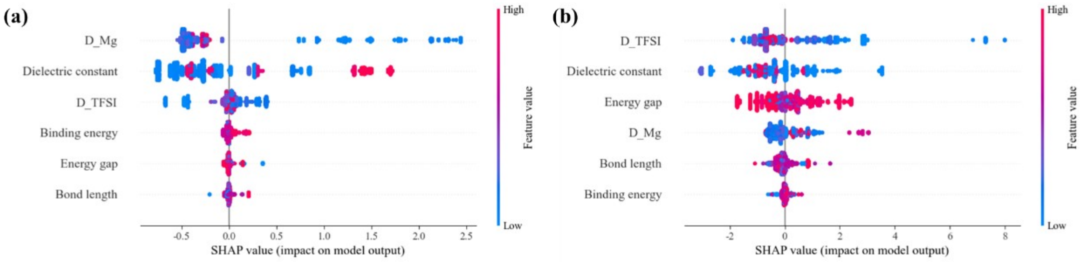

Figure S8. Shaply ordering of XGBOOST (a–b) models training on migration ML database with outputs of overpotential and cycle life.

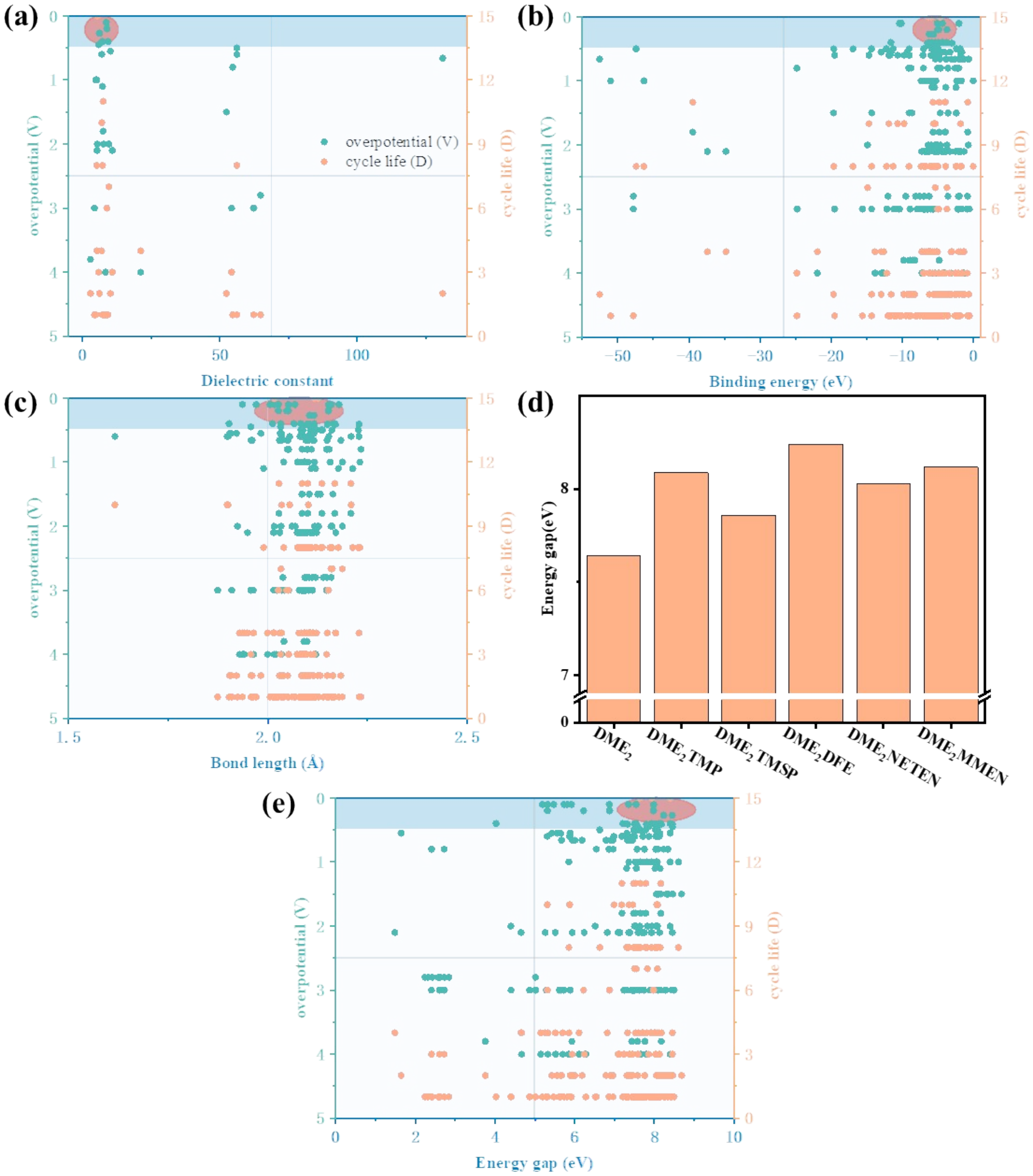

Figure S9. Relationship between dielectric constant (a), binding energy (b), bond length (c), energy gap (e) and electrochemical performance. d, Comparison of energy gap of solvation structure with P/N additives and pure solvent.

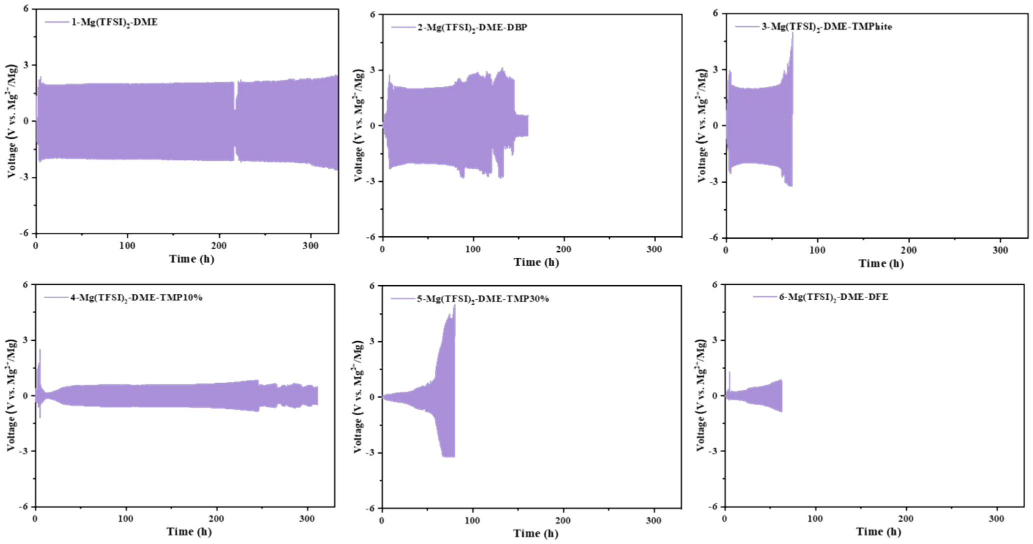
1-Mg(TFSI)$_2$-DME
2-Mg(TFSI)$_2$-DME-DBP
3-Mg(TFSI)$_2$-DME-TMPhite
4-Mg(TFSI)$_2$-DME-TMP10%
5-Mg(TFSI)$_2$-DME-TMP30%
6-Mg(TFSI)$_2$-DME-DFE
Voltage (V vs. Mg$^{2+}$/Mg)
Time (h)
6
3
0
-3
-6
0
100
200
300

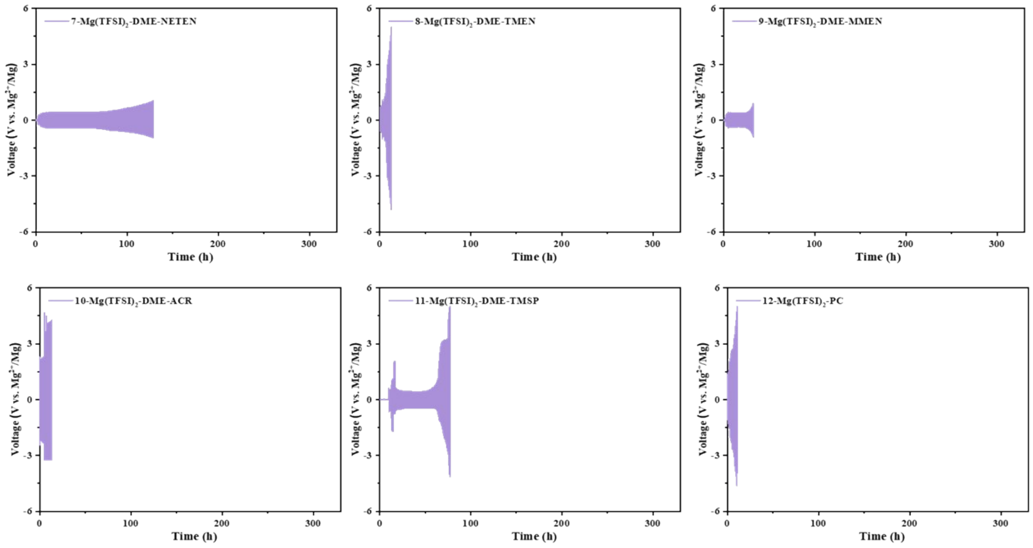
7-Mg(TFSI)$_2$-DME-NETEN
8-Mg(TFSI)$_2$-DME-TMEN
9-Mg(TFSI)$_2$-DME-MMEN
10-Mg(TFSI)$_2$-DME-ACR
11-Mg(TFSI)$_2$-DME-TMSP
12-Mg(TFSI)$_2$-PC
Voltage (V vs. Mg$^{2+}$/Mg)
Time (h)
6
3
0
-3
-6
0
100
200
300

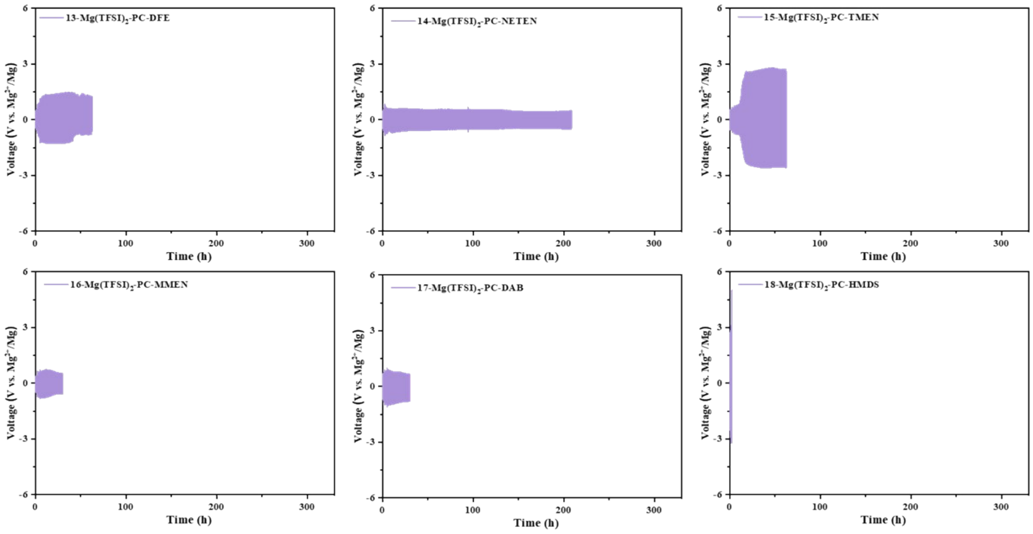
13-Mg(TFSI)$_2$-PC-DFE
14-Mg(TFSI)$_2$-PC-NETEN
15-Mg(TFSI)$_2$-PC-TMEN
16-Mg(TFSI)$_2$-PC-MMEN
17-Mg(TFSI)$_2$-PC-DAB
18-Mg(TFSI)$_2$-PC-HMDS
Voltage (V vs. Mg$^{2+}$/Mg)
Time (h)
6
3
0
-3
-6
0
100
200
300

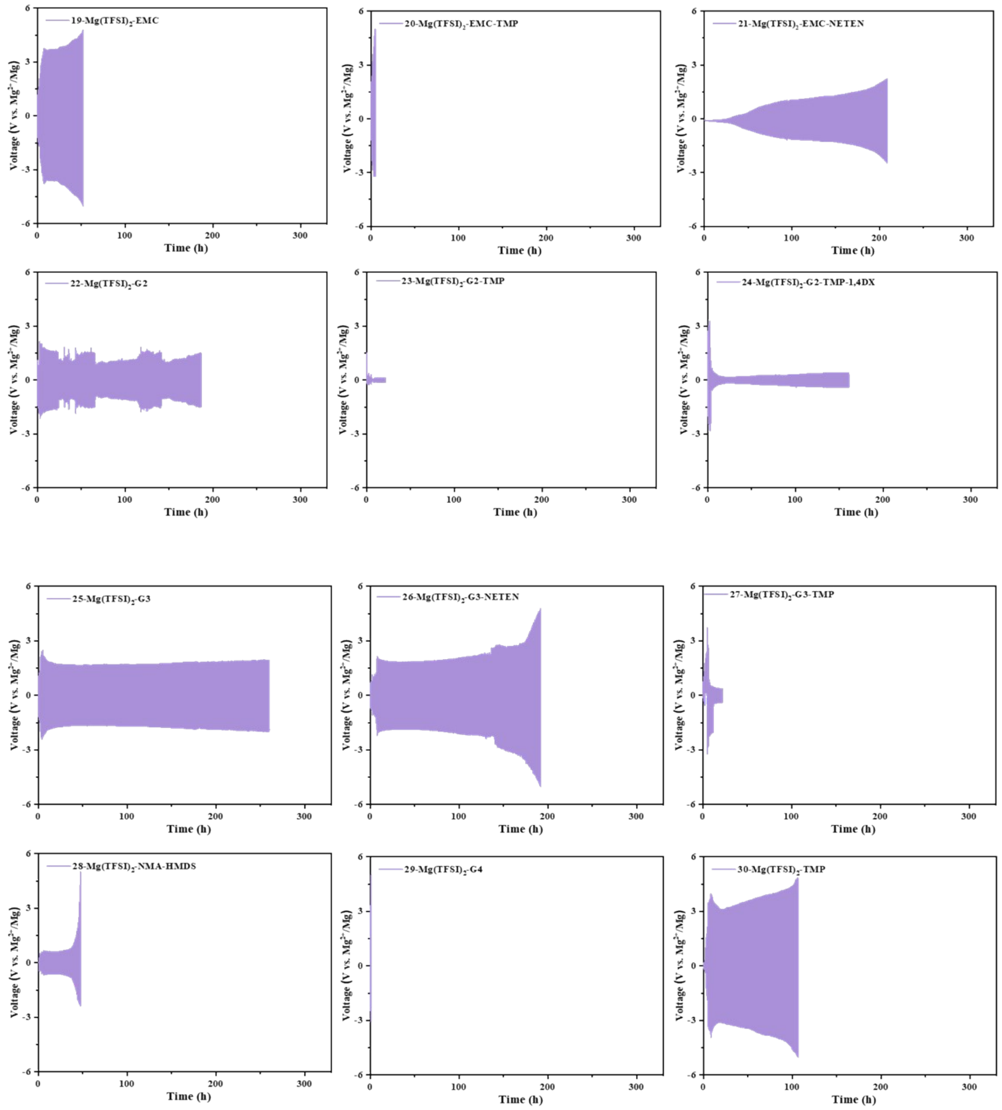

Figure S10. Galvanostatic cycling of Mg symmetric cells with 30 sets of electrolyte formulations at a current density of 0.1 mA cm$^{-2}$.

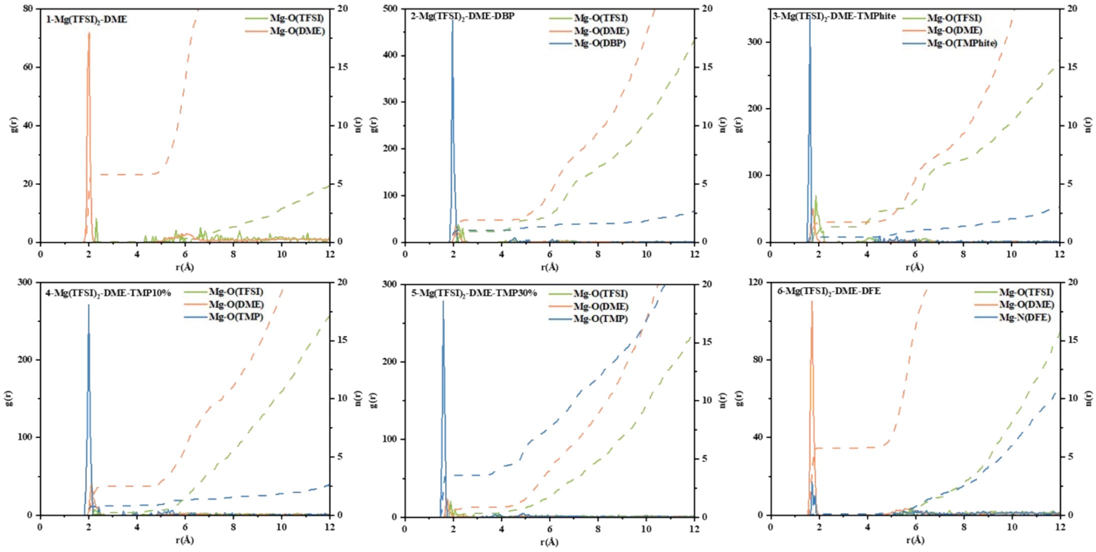

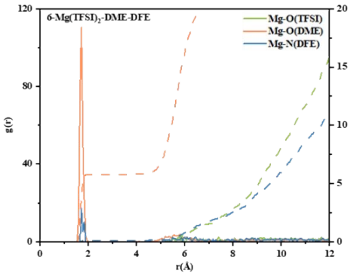
6-Mg(TFSI)$_2$-DME-DFE
Mg-O(TFSI)
Mg-O(DME)
Mg-N(DFE)
g(r)
n(r)
r(Å)

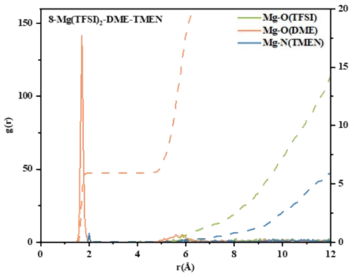
8-Mg(TFSI)$_2$-DME-TMEN
Mg-O(TFSI)
Mg-O(DME)
Mg-N(TMEN)
g(r)
n(r)
r(Å)

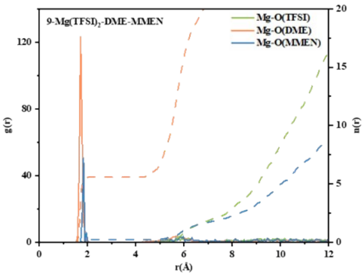
9-Mg(TFSI)$_2$-DME-MMEN
Mg-O(TFSI)
Mg-O(DME)
Mg-O(MMEN)
g(r)
n(r)
r(Å)

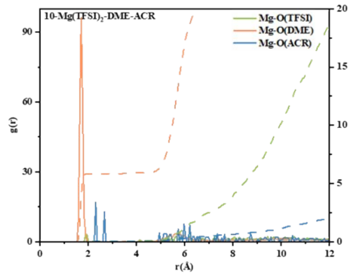
10-Mg(TFSI)$_2$-DME-ACR
Mg-O(TFSI)
Mg-O(DME)
Mg-O(ACR)
g(r)
n(r)
r(Å)

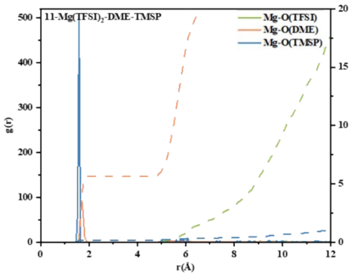
11-Mg(TFSI)$_2$-DME-TMSP
Mg-O(TFSI)
Mg-O(DME)
Mg-O(TMSP)
g(r)
n(r)
r(Å)

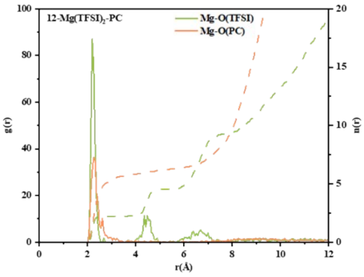
12-Mg(TFSI)$_2$-PC
Mg-O(TFSI)
Mg-O(PC)
g(r)
n(r)
r(Å)

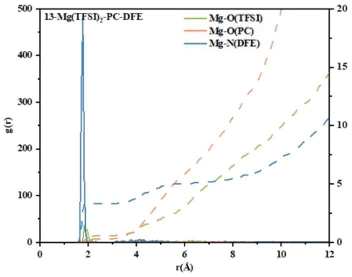
13-Mg(TFSI)$_2$-PC-DFE
Mg-O(TFSI)
Mg-O(PC)
Mg-N(DFE)
g(r)
n(r)
r(Å)

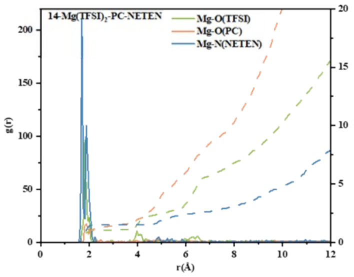
14-Mg(TFSI)$_2$-PC-NETEN
Mg-O(TFSI)
Mg-O(PC)
Mg-N(NETEN)
g(r)
n(r)
r(Å)

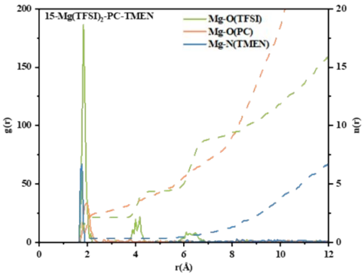
15-Mg(TFSI)$_2$-PC-TMEN
Mg-O(TFSI)
Mg-O(PC)
Mg-N(TMEN)
g(r)
n(r)
r(Å)

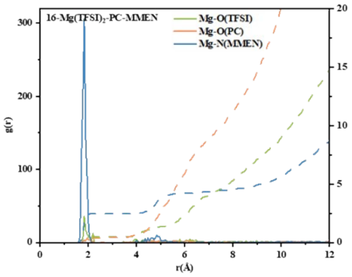
16-Mg(TFSI)$_2$-PC-MMEN
Mg-O(TFSI)
Mg-O(PC)
Mg-N(MMEN)
g(r)
n(r)
r(Å)

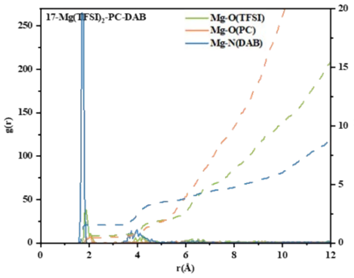
17-Mg(TFSI)$_2$-PC-DAB
Mg-O(TFSI)
Mg-O(PC)
Mg-N(DAB)
g(r)
n(r)
r(Å)

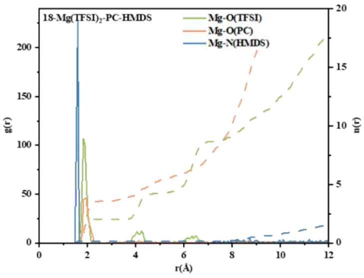
18-Mg(TFSI)$_2$-PC-HMDS
Mg-O(TFSI)
Mg-O(PC)
Mg-N(HMDS)
g(r)
n(r)
r(Å)

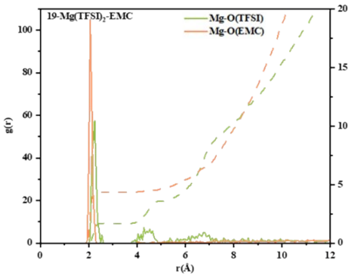
19-Mg(TFSI)$_2$-EMC
Mg-O(TFSI)
Mg-O(EMC)
g(r)
n(r)
r(Å)

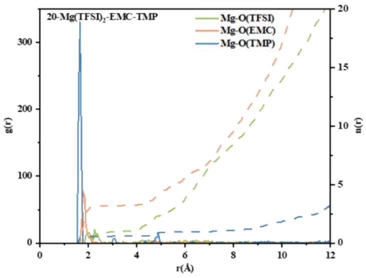
20-Mg(TFSI)$_2$-EMC-TMP
Mg-O(TFSI)
Mg-O(EMC)
Mg-O(TMP)
g(r)
n(r)
r(Å)

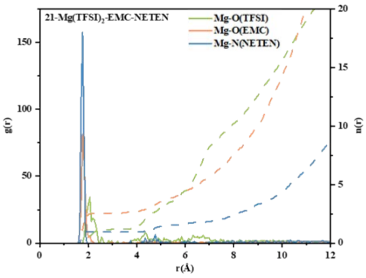
21-Mg(TFSI)$_2$-EMC-NETEN
Mg-O(TFSI)
Mg-O(EMC)
Mg-N(NETEN)
g(r)
n(r)
r(Å)

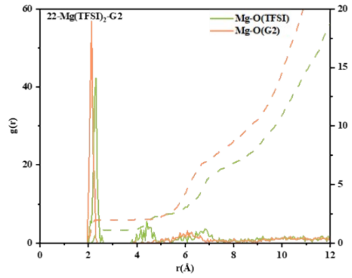
22-Mg(TFSI)$_2$-G2
Mg-O(TFSI)
Mg-O(G2)
g(r)
n(r)
r(Å)

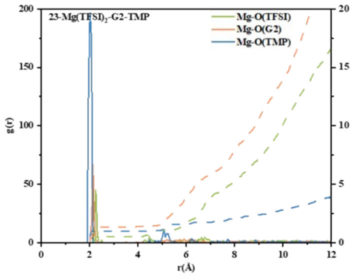
23-Mg(TFSI)$_2$-G2-TMP
Mg-O(TFSI)
Mg-O(G2)
Mg-O(TMP)
g(r)
n(r)
r(Å)

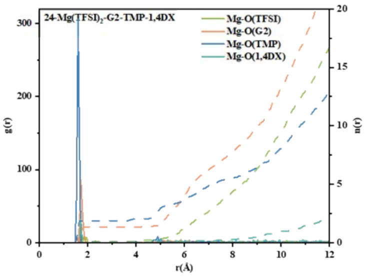
24-Mg(TFSI)$_2$-G2-TMP-1,4DX
Mg-O(TFSI)
Mg-O(G2)
Mg-O(TMP)
Mg-O(1,4DX)
g(r)
n(r)
r(Å)

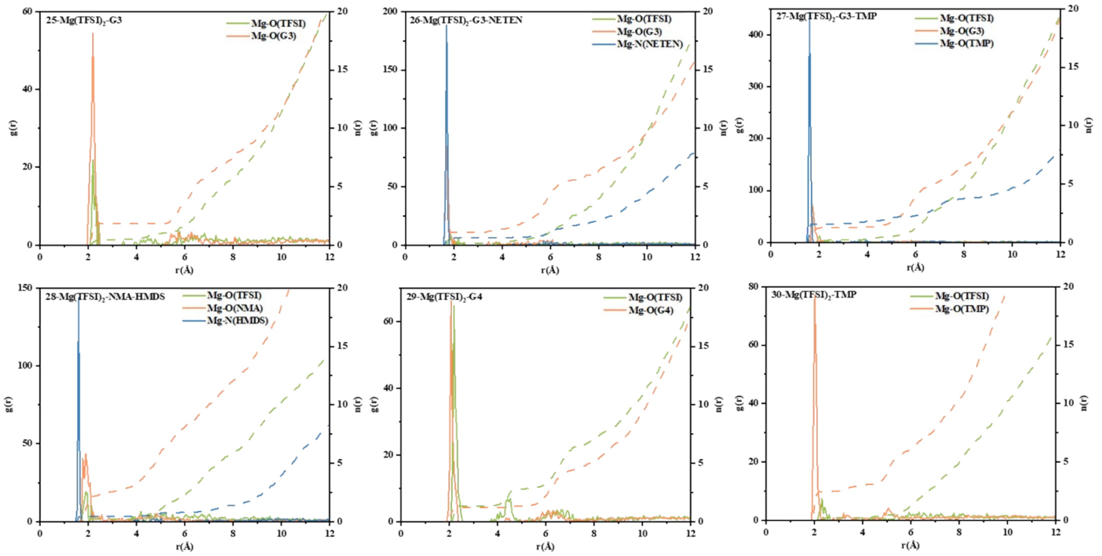

Figure S11. Radial distribution functions (g(r), solid line) and coordination number (n(r), dashed line) of oxygen from TFSI⁻, and oxygen or nitrogen from solvent around $Mg^{2+}$ in 30 sets of electrolyte formulations from molecular dynamic simulations.

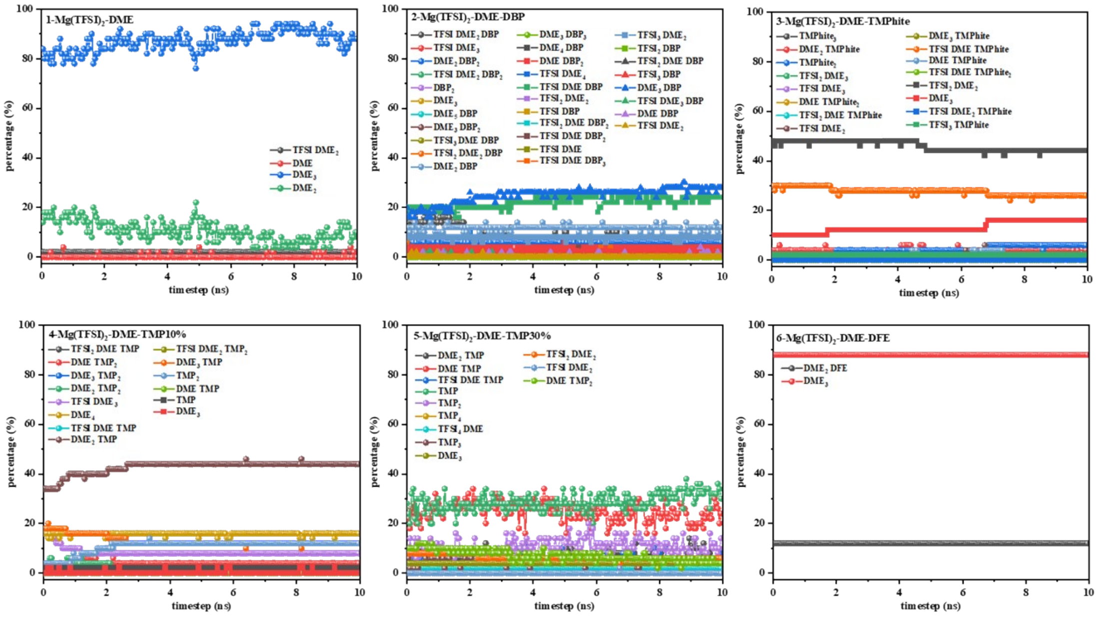

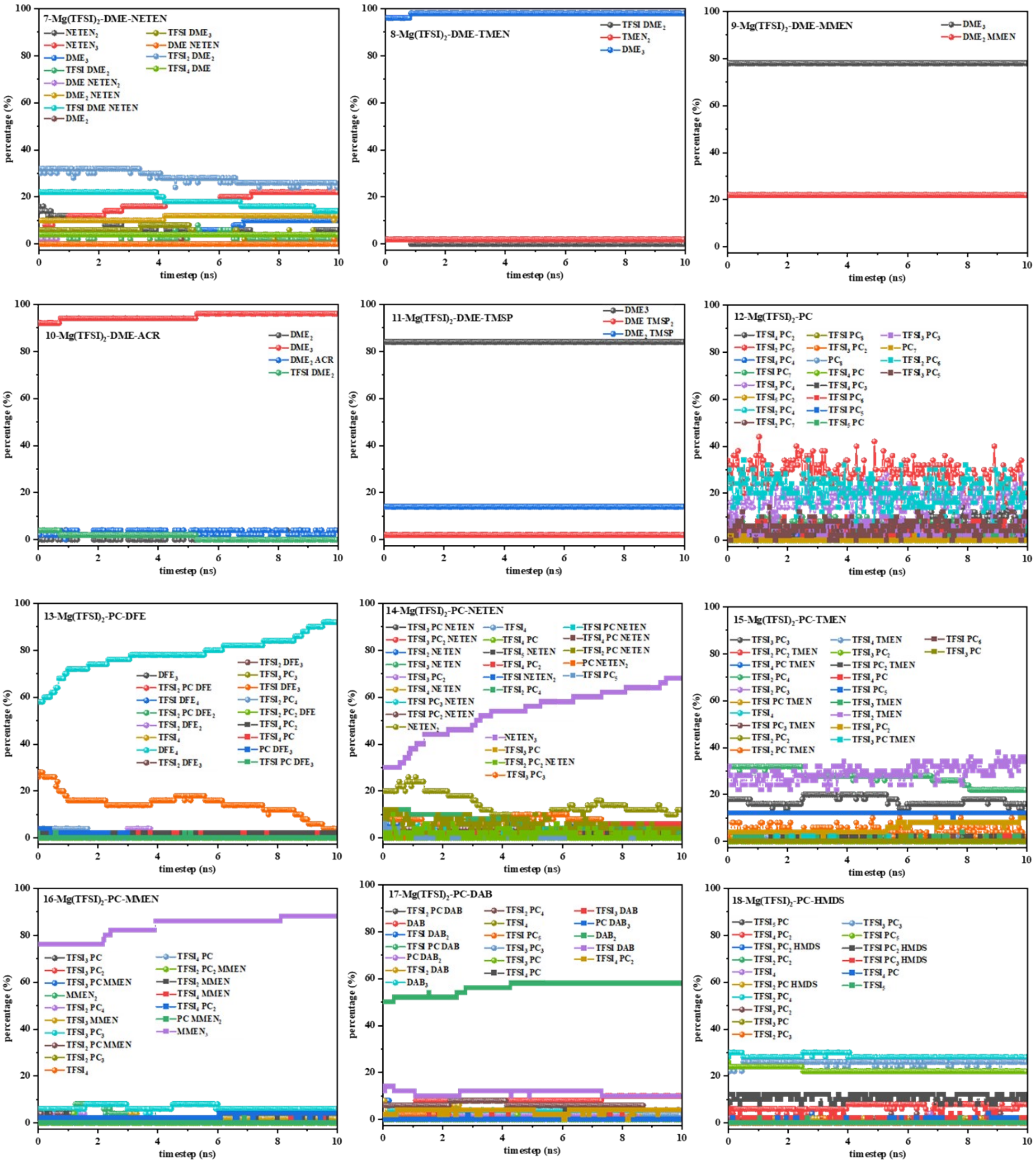
7-Mg(TFSI)$_2$-DME-NETEN
NETEN$_2$
NETEN$_3$
DME$_3$
TFSI DME$_2$
DME NETEN$_2$
DME$_2$ NETEN
TFSI DME NETEN
DME$_2$
TFSI DME$_3$
DME NETEN
TFSI$_2$ DME$_2$
TFSI$_4$ DME
8-Mg(TFSI)$_2$-DME-TMEN
TFSI DME$_2$
TMEN$_2$
DME$_3$
9-Mg(TFSI)$_2$-DME-MMEN
DME$_3$
DME$_2$ MMEN
10-Mg(TFSI)$_2$-DME-ACR
DME$_2$
DME$_3$
DME$_2$ ACR
TFSI DME$_2$
11-Mg(TFSI)$_2$-DME-TMSP
DME3
DME TMSP$_2$
DME$_2$ TMSP
12-Mg(TFSI)$_2$-PC
TFSI$_4$ PC$_2$
TFSI$_2$ PC$_5$
TFSI$_4$ PC$_4$
TFSI PC$_7$
TFSI$_3$ PC$_4$
TFSI$_5$ PC$_2$
TFSI$_2$ PC$_4$
TFSI$_2$ PC$_7$
TFSI PC$_8$
TFSI$_3$ PC$_2$
PC$_8$
TFSI$_4$ PC
TFSI$_4$ PC$_3$
TFSI PC$_6$
TFSI PC$_5$
TFSI$_5$ PC
TFSI$_3$ PC$_3$
PC$_7$
TFSI$_2$ PC$_6$
TFSI$_3$ PC$_5$
13-Mg(TFSI)$_2$-PC-DFE
DFE$_3$
TFSI$_2$ PC DFE
TFSI DFE$_4$
TFSI$_2$ PC DFE$_2$
TFSI$_2$ DFE$_2$
TFSI$_4$
DFE$_4$
TFSI$_2$ DFE$_3$
TFSI$_2$ DFE$_3$
TFSI$_3$ PC$_3$
TFSI DFE$_3$
TFSI$_2$ PC$_4$
TFSI$_2$ PC$_2$ DFE
TFSI$_4$ PC$_2$
TFSI$_4$ PC
PC DFE$_3$
TFSI PC DFE$_3$
14-Mg(TFSI)$_2$-PC-NETEN
TFSI$_3$ PC NETEN
TFSI$_3$ PC$_2$ NETEN
TFSI$_2$ NETEN
TFSI$_3$ NETEN
TFSI$_3$ PC$_2$
TFSI$_4$ NETEN
TFSI PC$_3$ NETEN
TFSI PC$_2$ NETEN
NETEN$_2$
TFSI$_4$
TFSI$_4$ PC
TFSI$_5$ NETEN
TFSI$_4$ PC$_2$
TFSI NETEN$_2$
TFSI$_2$ PC$_4$
TFSI PC NETEN
TFSI$_4$ PC NETEN
TFSI$_2$ PC NETEN
PC NETEN$_2$
TFSI PC$_5$
NETEN$_3$
TFSI$_3$ PC
TFSI$_2$ PC$_2$ NETEN
TFSI$_3$ PC$_3$
15-Mg(TFSI)$_2$-PC-TMEN
TFSI$_3$ PC$_3$
TFSI$_2$ PC$_2$ TMEN
TFSI$_4$ PC TMEN
TFSI$_2$ PC$_4$
TFSI$_2$ PC$_3$
TFSI PC TMEN
TFSI$_4$
TFSI PC$_3$ TMEN
TFSI$_3$ PC$_2$
TFSI$_2$ PC TMEN
TFSI$_4$ TMEN
TFSI$_3$ PC$_2$
TFSI PC$_2$ TMEN
TFSI$_4$ PC
TFSI PC$_5$
TFSI$_3$ TMEN
TFSI$_2$ TMEN
TFSI$_4$ PC$_2$
TFSI$_3$ PC TMEN
TFSI PC$_6$
TFSI$_3$ PC
16-Mg(TFSI)$_2$-PC-MMEN
TFSI$_3$ PC
TFSI$_3$ PC$_2$
TFSI$_3$ PC MMEN
MMEN$_2$
TFSI$_2$ PC$_4$
TFSI$_3$ MMEN
TFSI$_3$ PC$_3$
TFSI$_2$ PC MMEN
TFSI$_2$ PC$_3$
TFSI$_4$
TFSI$_4$ PC
TFSI$_2$ PC$_2$ MMEN
TFSI$_2$ MMEN
TFSI$_4$ MMEN
TFSI$_4$ PC$_2$
PC MMEN$_2$
MMEN$_3$
17-Mg(TFSI)$_2$-PC-DAB
TFSI$_2$ PC DAB
DAB
TFSI DAB$_2$
TFSI PC DAB
PC DAB$_2$
TFSI$_2$ DAB
DAB$_3$
TFSI$_2$ PC$_4$
TFSI$_4$
TFSI PC$_5$
TFSI$_3$ PC$_3$
TFSI$_3$ PC
TFSI$_4$ PC
TFSI$_3$ DAB
PC DAB$_3$
DAB$_2$
TFSI DAB
TFSI$_4$ PC$_2$
18-Mg(TFSI)$_2$-PC-HMDS
TFSI$_5$ PC
TFSI$_4$ PC$_2$
TFSI$_2$ PC$_2$ HMDS
TFSI$_2$ PC$_2$
TFSI$_4$
TFSI$_2$ PC HMDS
TFSI$_2$ PC$_4$
TFSI$_3$ PC$_2$
TFSI$_3$ PC
TFSI$_2$ PC$_3$
TFSI$_3$ PC$_3$
TFSI PC$_5$
TFSI PC$_2$ HMDS
TFSI PC$_3$ HMDS
TFSI$_4$ PC
TFSI$_5$
percentage (%)
timestep (ns)
0
2
4
6
8
10
0
20
40
60
80
100

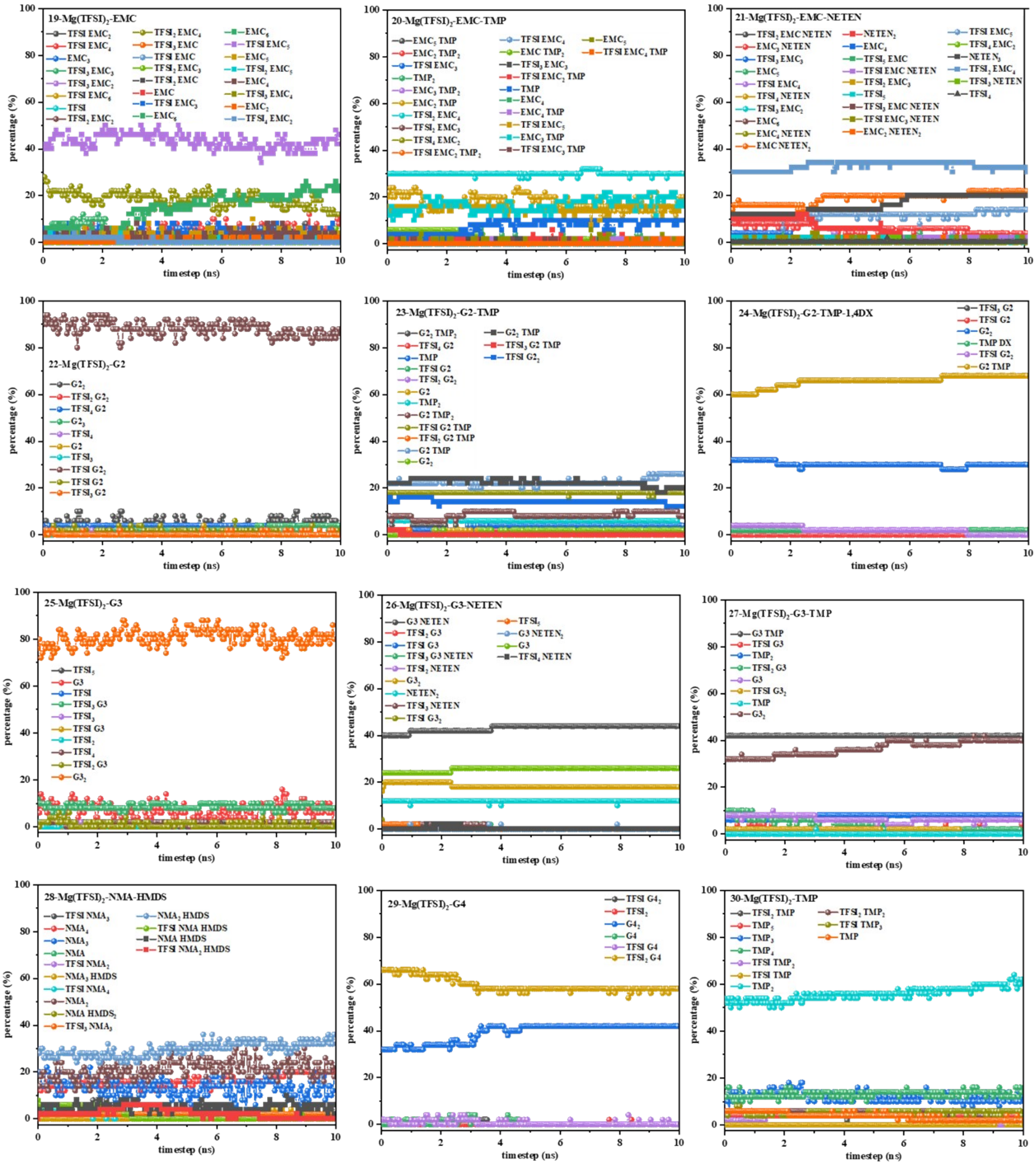

Figure S12. Molecular dynamics simulations of 30 sets of electrolyte formulations, equilibrated and run for 10 ns, with solvation structure percentage analyzed every 0.5 ns.

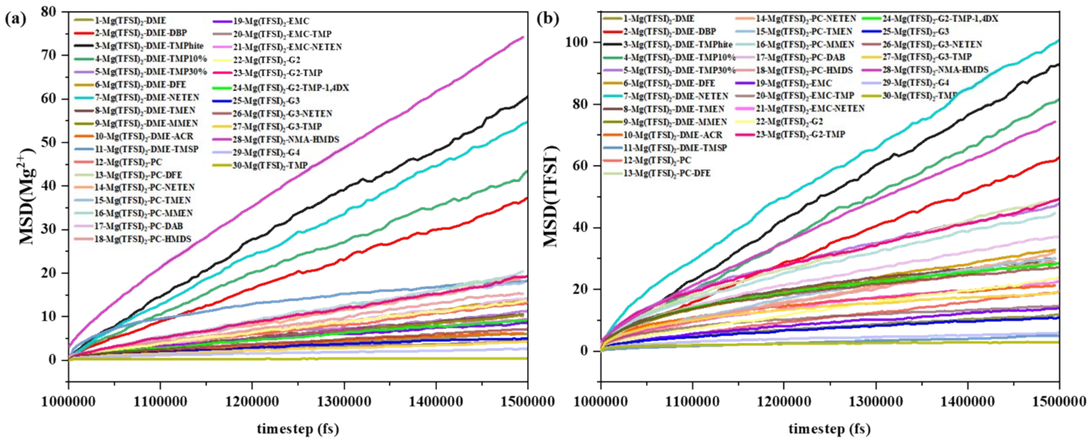

Figure S13. Molecular dynamics simulations of 30 sets of electrolyte formulations, equilibrated and run for 10 ns, with MSD calculated every 0.5 ns and averaged to obtain the MSD curve.

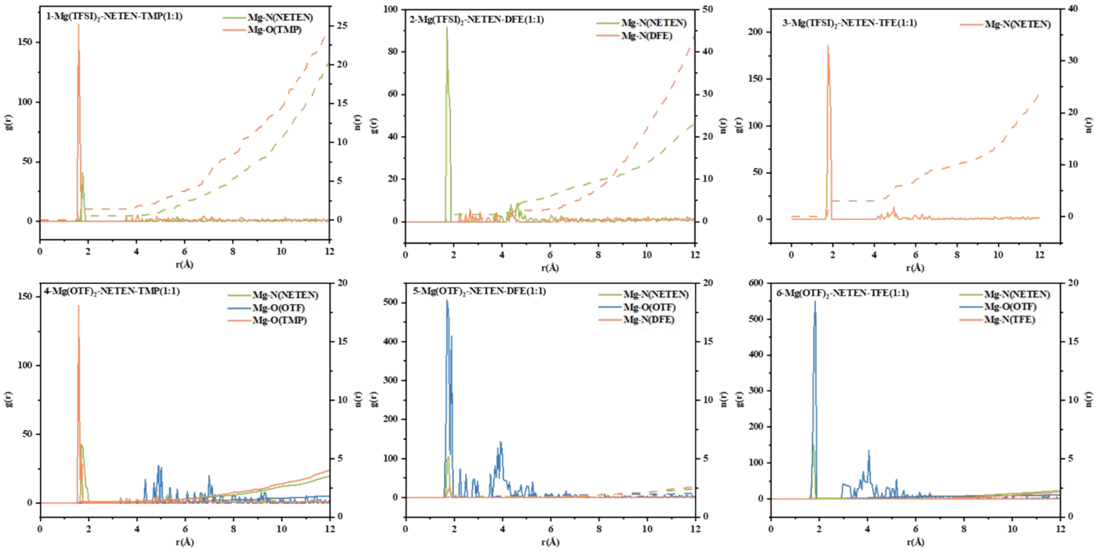

Figure S14. Radial distribution functions (g(r), solid lines) and coordination numbers (n(r), dashed lines) of oxygen from TFSI$^{-}$ or OTF$^{-}$ and oxygen or nitrogen from solvent around Mg$^{2+}$ in 6 test electrolyte formulations obtained from molecular dynamics simulations.

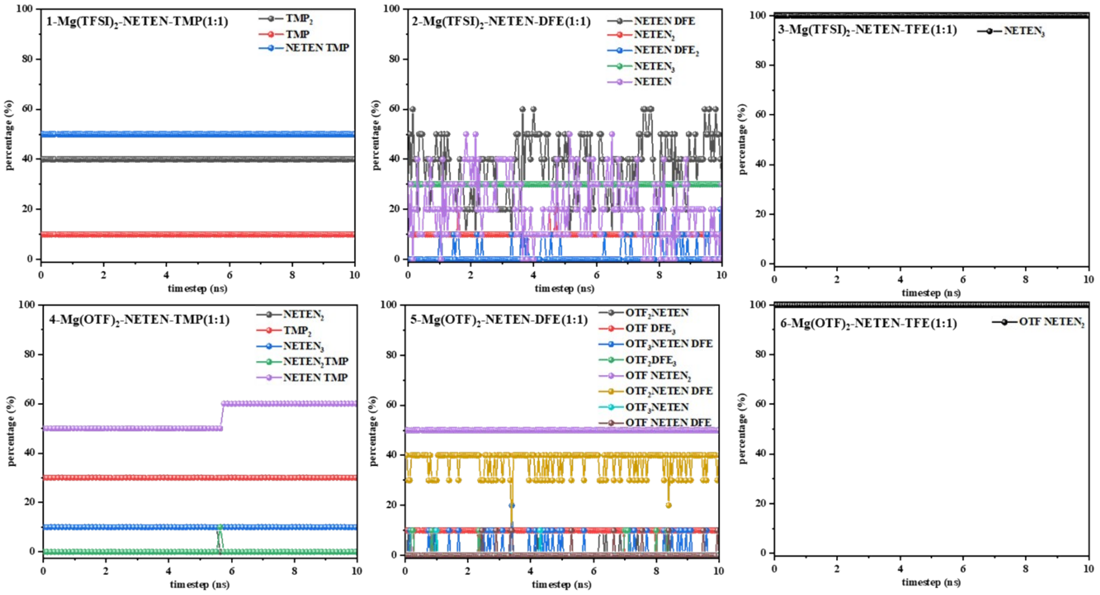

Figure S15. Molecular dynamics simulations of 6 test electrolyte formulations, equilibrated and run for 10 ns, with solvation structure percentage analyzed every 0.5 ns.

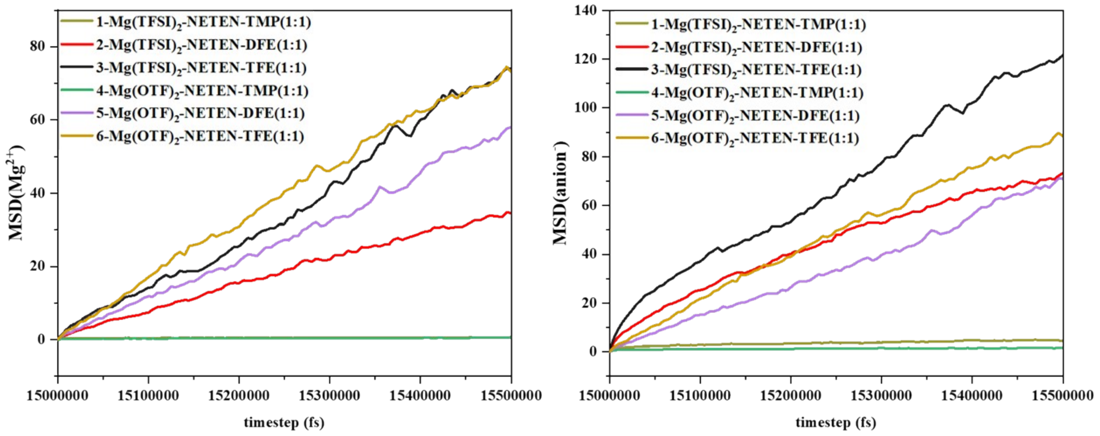

Figure S16. Molecular dynamics simulations of 6 test electrolyte formulations, equilibrated and run for 10 ns, with MSD calculated every 0.5 ns and averaged to obtain the MSD curve.

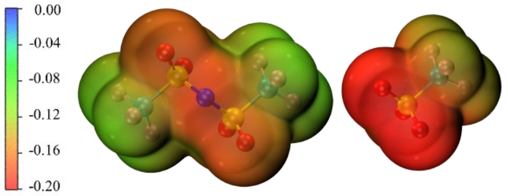

| Anion | Space size (Å) | ESP$_{min}$ (eV) | ESP$_{max}$ (eV) |
|---|---|---|---|
| TFSI$^-$ | 7.22×3.80×2.52 | -5.08 | -2.21 |
| OTF$^-$ | 3.02×2.50×2.50 | -5.38 | -3.02 |

Figure S17. Calculated electrostatic potential maps of TFSI$^-$ and OTF$^-$ under vacuum conditions.

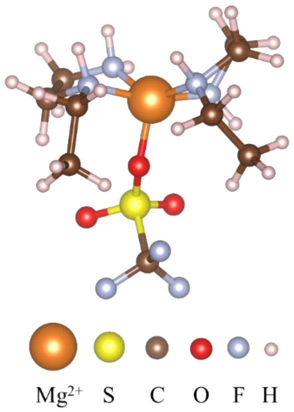

Figure S18. Solvated structures (OTF NETEN2) of NETEN+DFE–Mg(OTF)$_2$ and NETEN+TFE–Mg(OTF)$_2$.

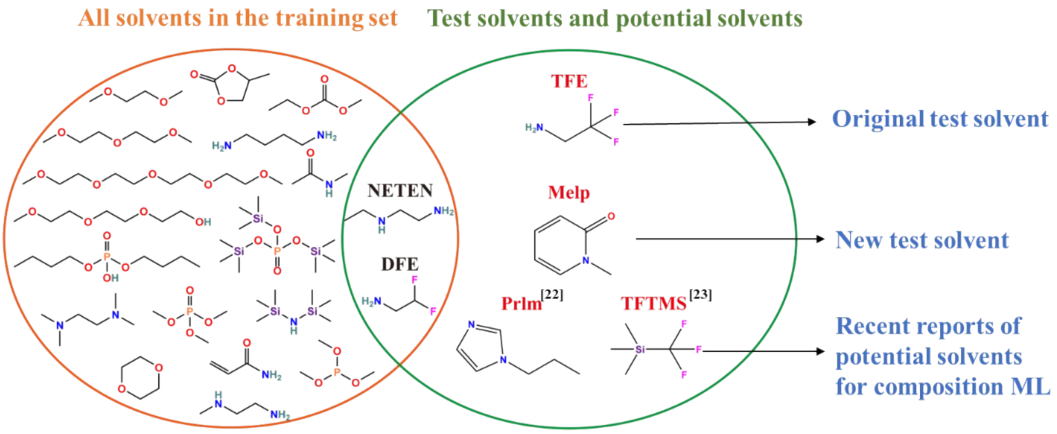

Figure S19. Similarity comparison of training set solvents and test solvents[22, 23].

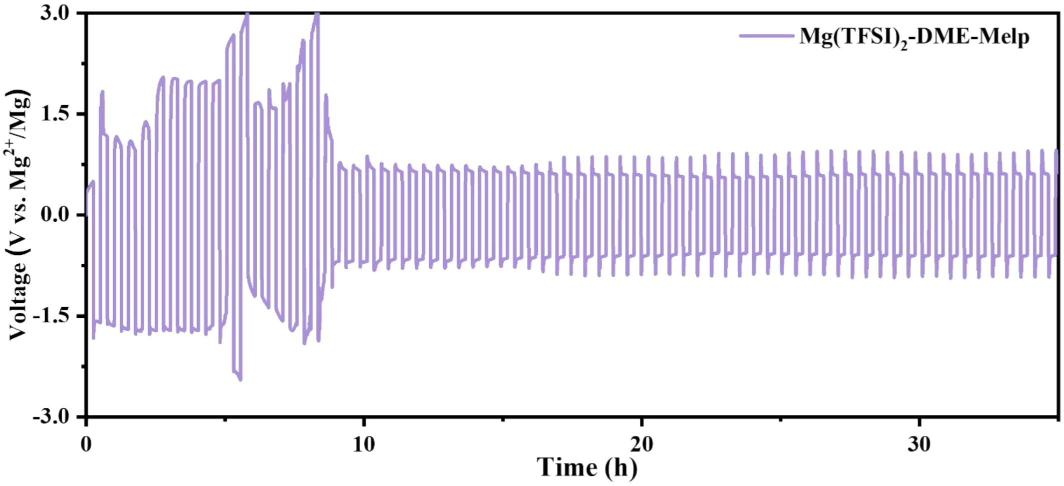

Figure S20. Galvanostatic cycling of Mg symmetric cells with $Mg(TFSI)_2$–DME–Melp electrolyte formulation at a current density of 0.1 mA cm$^{-2}$.

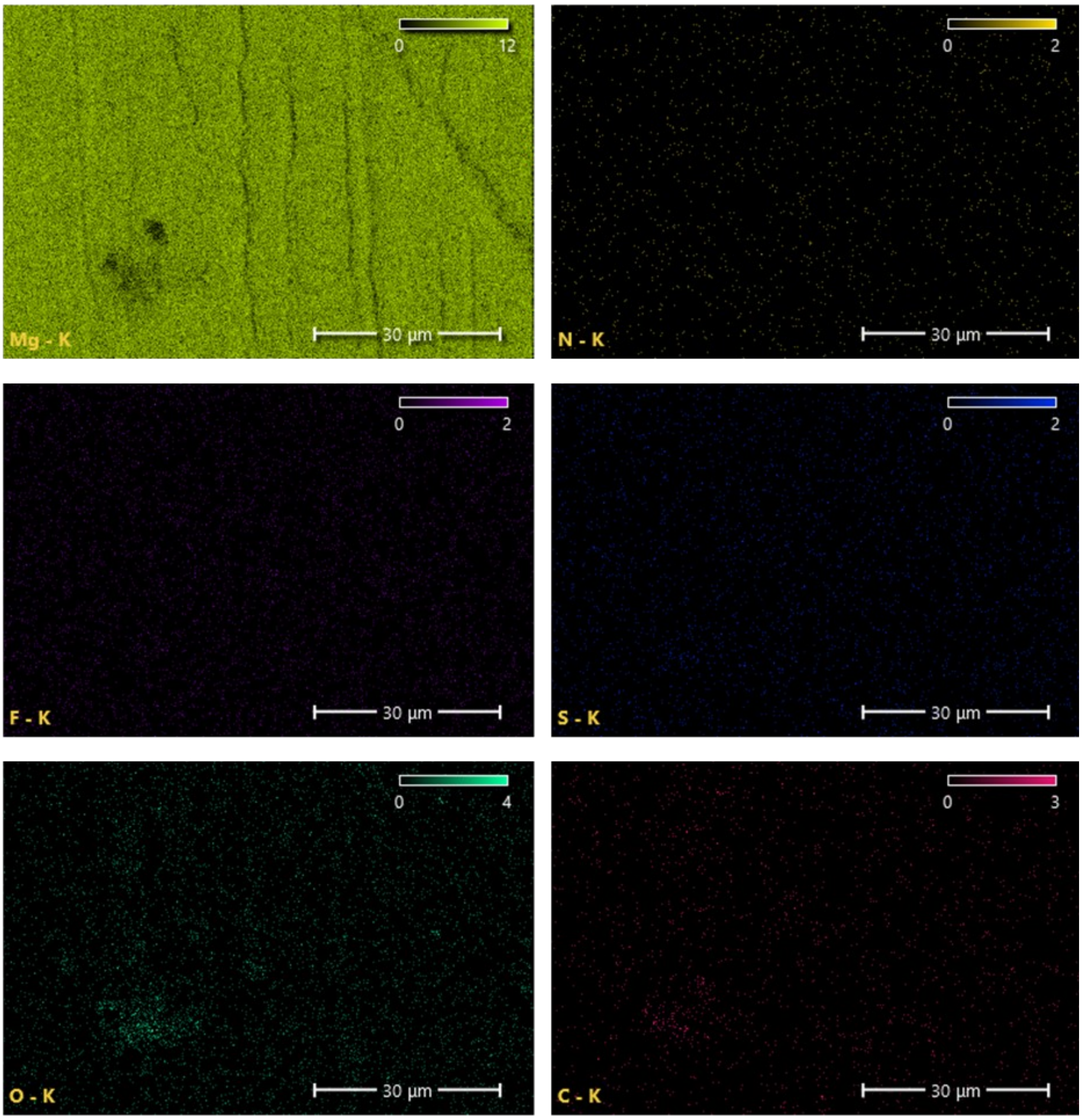

Figure S21. EDS results of the 20th cycled Mg anode surface in the NETEN+DFE–Mg(OTF)$_2$ electrolyte.

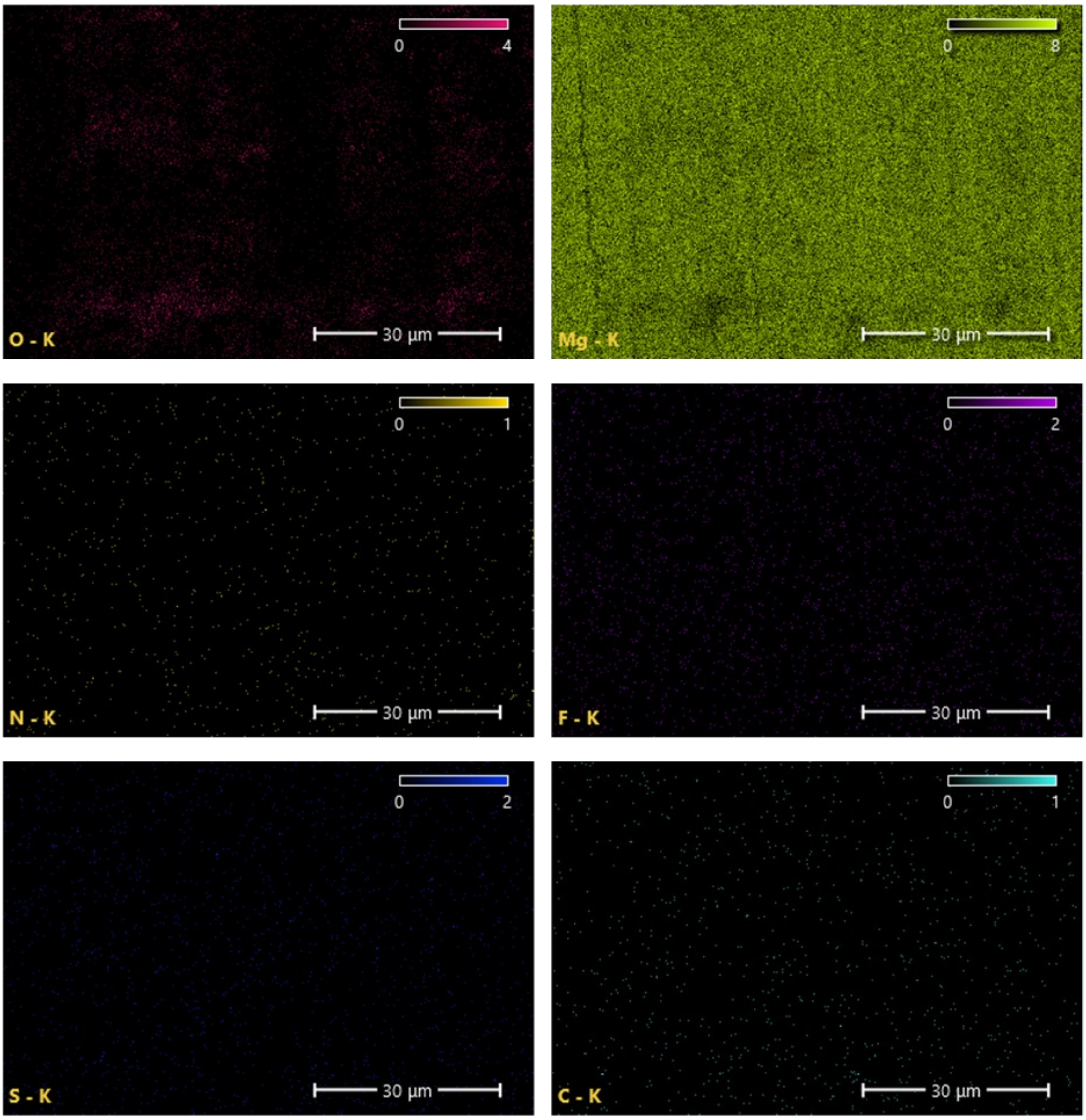

Figure S22. EDS results of the 20th cycled Mg anode surface in the NETEN+TFE–Mg(OTF)$_2$ electrolyte.

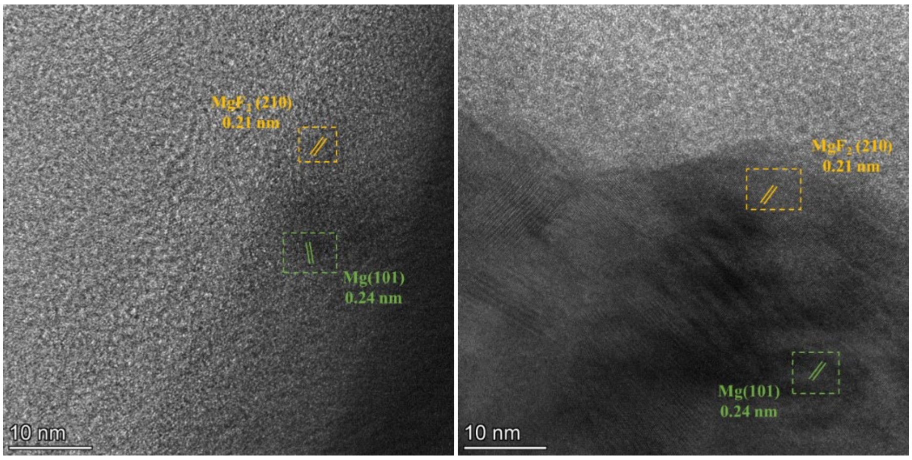

Figure S23. Nanostructure of Mg deposited in the NETEN+DFE–Mg(OTF)$_2$ and NETEN+TFE–Mg(OTF)$_2$ electrolytes imaged by TEM.

## IV. Supporting References

1. W. L. Jorgensen, D. S. Maxwell and J. Tirado-Rives, *Journal of the American Chemical Society*, 1996, **118**, 11225-11236.
2. W. L. Jorgensen and J. Tirado-Rives, *Proc Natl Acad Sci U S A*, 2005, **102**, 6665-6670.
3. L. S. Dodda, J. Z. Vilseck, J. Tirado-Rives and W. L. Jorgensen, *J Phys Chem B*, 2017, **121**, 3864-3870.
4. L. S. Dodda, I. Cabeza de Vaca, J. Tirado-Rives and W. L. Jorgensen, *Nucleic Acids Res*, 2017, **45**, W331-w336.
5. J. Wang, W. Wang, P. A. Kollman and D. A. Case, *J Mol Graph Model*, 2006, **25**, 247-260.
6. M. S. Kelkar and E. J. Maginn, *J Phys Chem B*, 2007, **111**, 4867-4876.
7. D. Beglov and B. Roux, *The Journal of Chemical Physics*, 1994, **100**, 9050-9063.
8. M. J. Frisch, G. W. Trucks, H. B. Schlegel, G. E. Scuseria, M. A. Robb, J. R. Cheeseman, G. Scalmani, V. Barone, G. A. Petersson, H. Nakatsuji, X. Li, M. Caricato, A. V. Marenich, J. Bloino, B. G. Janesko, R. Gomperts, B. Mennucci, H. P. Hratchian, J. V. Ortiz, A. F. Izmaylov, J. L. Sonnenberg, Williams, F. Ding, F. Lipparini, F. Egidi, J. Goings, B. Peng, A. Petrone, T. Henderson, D. Ranasinghe, V. G. Zakrzewski, J. Gao, N. Rega, G. Zheng, W. Liang, M. Hada, M. Ehara, K. Toyota, R. Fukuda, J. Hasegawa, M. Ishida, T. Nakajima, Y. Honda, O. Kitao, H. Nakai, T. Vreven, K. Throssell, J. A. Montgomery Jr., J. E. Peralta, F. Ogliaro, M. J. Bearpark, J. J. Heyd, E. N. Brothers, K. N. Kudin, V. N. Staroverov, T. A. Keith, R. Kobayashi, J. Normand, K. Raghavachari, A. P. Rendell, J. C. Burant, S. S. Iyengar, J. Tomasi, M. Cossi, J. M. Millam, M. Klene, C. Adamo, R. Cammi, J. W. Ochterski, R. L. Martin, K. Morokuma, O. Farkas, J. B. Foresman and D. J. Fox, *Journal*, 2016.
9. A. D. Becke, *The Journal of Chemical Physics*, 1993, **98**, 5648-5652.
10. A. V. Marenich, C. J. Cramer and D. G. Truhlar, *The Journal of Physical Chemistry B*, 2009, **113**, 6378-6396.
11. A. E. Reed, L. A. Curtiss and F. Weinhold, *Chemical Reviews*, 1988, **88**, 899-926.
12. T. Lu and F. Chen, *J Comput Chem*, 2012, **33**, 580-592.
13. A. Swami and R. Jain, *Journal of Machine Learning Research*, 2013, **12**, 2825-2830.
14. O. Allam, R. Kuramshin, Z. Stoichev, B. W. Cho, S. W. Lee and S. S. Jang, *Materials Today Energy*, 2020, **17**, 100482.
15. Y. Okamoto and Y. Kubo, *ACS Omega*, 2018, **3**, 7868-7874.
16. Y. Zhuo, A. Mansouri Tehrani and J. Brgoch, *The Journal of Physical Chemistry Letters*, 2018, **9**, 1668-1673.
17. Y.-C. Gao, N. Yao, X. Chen, L. Yu, R. Zhang and Q. Zhang, *Journal of the American Chemical Society*, 2023, **145**, 23764-23770.

18. S. C. Kim, S. T. Oyakhire, C. Athanitis, J. Wang, Z. Zhang, W. Zhang, D. T. Boyle, M. S. Kim, Z. Yu, X. Gao, T. Sogade, E. Wu, J. Qin, Z. Bao, S. F. Bent and Y. Cui, *Proceedings of the National Academy of Sciences*, 2023, **120**, e2214357120.
19. P. Liu, Y. Wen, L. Huang, X. Zhu, R. Wu, S. Ai, T. Xue and Y. Ge, *Journal of Electroanalytical Chemistry*, 2021, **899**, 115684.
20. E. Štrumbelj and I. Kononenko, *Knowledge and Information Systems*, 2014, **41**, 647-665.
21. S. M. Lundberg and S.-I. Lee, presented in part at the Proceedings of the 31st International Conference on Neural Information Processing Systems, Long Beach, California, USA, 2017.
22. A. Yang, X. Gao, M. Pei, J. Zhou, H. Wang, C. Liao, J. Xiao, Y. Liu, W. Yan and J. Zhang, *Angewandte Chemie International Edition*, 2025, **n/a**, e202424237.
23. Z. Fan, W. Zhao, S. Shi, M. Zhou, J. Li, Y. Liu, Z. Pan and X. Yang, *Angewandte Chemie International Edition*, 2025, **64**, e202416582.